Seismic-petrophysical reservoir characterization in the northern part of the Chicontepec Basin, Mexico

Supratik Sarkar[1], Sumit Verma[2], and Kurt J. Marfurt[2]

Abstract

The Chicontepec Formation in east-central Mexico is comprised of complex unconventional reservoirs consisting of low-permeability disconnected turbidite reservoir facies. Hydraulic fracturing increases permeability and joins these otherwise tight reservoirs. We use a recently acquired 3D seismic survey and well control to divide the Chicontepec reservoir interval in the northern part of the basin into five stratigraphic units, equivalent to global third-order seismic sequences. By combining well-log and core information with principles of seismic geomorphology, we are able to map deepwater facies within these stratigraphic units that resulted from the complex interaction of flows from different directions. Correlating these stratigraphic units to producing and nonproducing wells provides the link between rock properties and Chicontepec reservoirs that could be delineated from surface seismic data. The final product is a prestack inversion-driven map of stacked pay that correlates to currently producing wells and indicates potential untapped targets.

Introduction

The sandstones in the Chicontepec Formation were deposited within a foredeep basin deepwater system during the Upper Paleocene and Early-Middle Eocene periods. The elongated foredeep basin is known as the Chicontepec foredeep, which was formed in front of the Sierra Madre Oriental (SMO) fold and thrust belt during the Late Cretaceous to Early Tertiary Laramide orogeny in east-central Mexico. The foredeep is bounded on the east by the Golden Lane atoll Cretaceous carbonate platform (Figure 1a and 1c).

The Chicontepec play is characterized by a complex depositional history, which can be attributed to the interplay of several factors, including multiple provenances, tectonic activity, and associated differential rate of subsidence and sediment accumulation within the foredeep. The deposits are rich in carbonate fragments eroded from nearby Jurassic and Cretaceous carbonate rocks spread throughout the region. Other than carbonate rock fragments, the major constituent is quartz along with feldspars and some clay. The Chicontepec sandstones have average quartz, feldspar, and rock fragment composition of $Q_{29}F_{13}R_{58}$ in the northern part of the Chicontepec Basin (Bermúdez et al., 2006). After the depositional events, the Chicontepec sandstone was subjected to extensive complex diagenetic processes (Bermúdez et al., 2006) and tertiary volcanic activity. The extensive carbonate cementation seen in the Chicontepec rocks is due to the presence of carbonate rock fragments as a major constituent.

The Chicontepec reservoirs have very low porosity (0.5%–11%) and permeability (0.001–5 mD). Factors contributing to this low porosity and permeability of the reservoir include poor sorting, predominance of carbonate rock fragments, and extensive diagenesis. Due to this poor reservoir quality, only 0.1% of the original oil in place, equal to 140 million barrels of oil-equivalent, had been recovered by 2002 (Cheatwood and Guzmán, 2002). Currently, production from the Chicontepec Formation in the Tampico-Misantla Basin occurs from some 50 fields scattered throughout the basin at depths ranging between 800 and 2400 m (Cossey, 2008).

The Chicontepec Formation and tight gas reservoirs in general do not exhibit a significant seismic "direct hydrocarbon indicator." In addition to the very low porosity and permeability of the reservoirs, the absence of free gas and the presence of large amounts of carbonate give rise to reservoirs that are relatively fluid insensitive, with almost no amplitude variation with offset (AVO) effect. We concentrate our study in the northern part of the Chicontepec foredeep, where prestack and poststack seismic data over an approximately 700 km^2 area (Figure 1a) are available along with well-logs and production data from oil fields situated in the eastern part of the sur-

[1]Formerly University of Oklahoma, School of Geology and Geophysics, Norman, Oklahoma, USA; presently Shell Exploration and Production Co., Houston, Texas, USA. E-mail: sarkar.supratik@gmail.com.

[2]University of Oklahoma, School of Geology and Geophysics, Norman, Oklahoma, USA. E-mail: sumit.verma.geophysicist@gmail.com; kmarfurt@ou.edu.

Manuscript received by the Editor 5 October 2015; revised manuscript received 2 February 2016; published online 18 July 2016. This paper appears in *Interpretation*, Vol. 4, No. 3 (August 2016); p. T403–T417, 15 FIGS., 1 TABLE.

http://dx.doi.org/10.1190/INT-2015-0168.1.

vey. The seismic data set is plagued by multiple shallow volcanic bodies, which give rise to velocity pull-up and interbed multiples. Extrusive volcanic mounds, swamps, and populated areas limit surface access, resulting in locally low-fold data (Figure 1b). As a result of these limitations to seismic data quality and the complex sediment stacking pattern, seismic data have played a minimal role in guiding the dense drilling program. Pemex had a 1000 new well-drilling program in 2009 (Donnelly, 2009), mostly guided by pattern drilling. Such challenges have been faced by other tight sandstone reservoirs as well. For example, a similar pattern drilling program has been conducted in the tight gas reservoirs in Wamsutter field, Wyoming; recently, however, advancements in geosciences have contributed to higher production and recovery rates in that area (Tobin et al., 2010; Geetan et al., 2011).

In this paper, we present a simple and effective way to characterize the complex unconventional Chicontepec reservoirs by integrating acoustic- and elastic-rock properties within a stratigraphic framework to better map the distribution of the potential reservoir units. We begin by building a geologic framework and delineating facies patterns for the Chicontepec reservoirs within the Amatitlan 3D seismic survey area. Then, we analyze the petrophysical properties from the well-logs and identify the set of properties that provides the best distinction between reservoir and nonreservoir

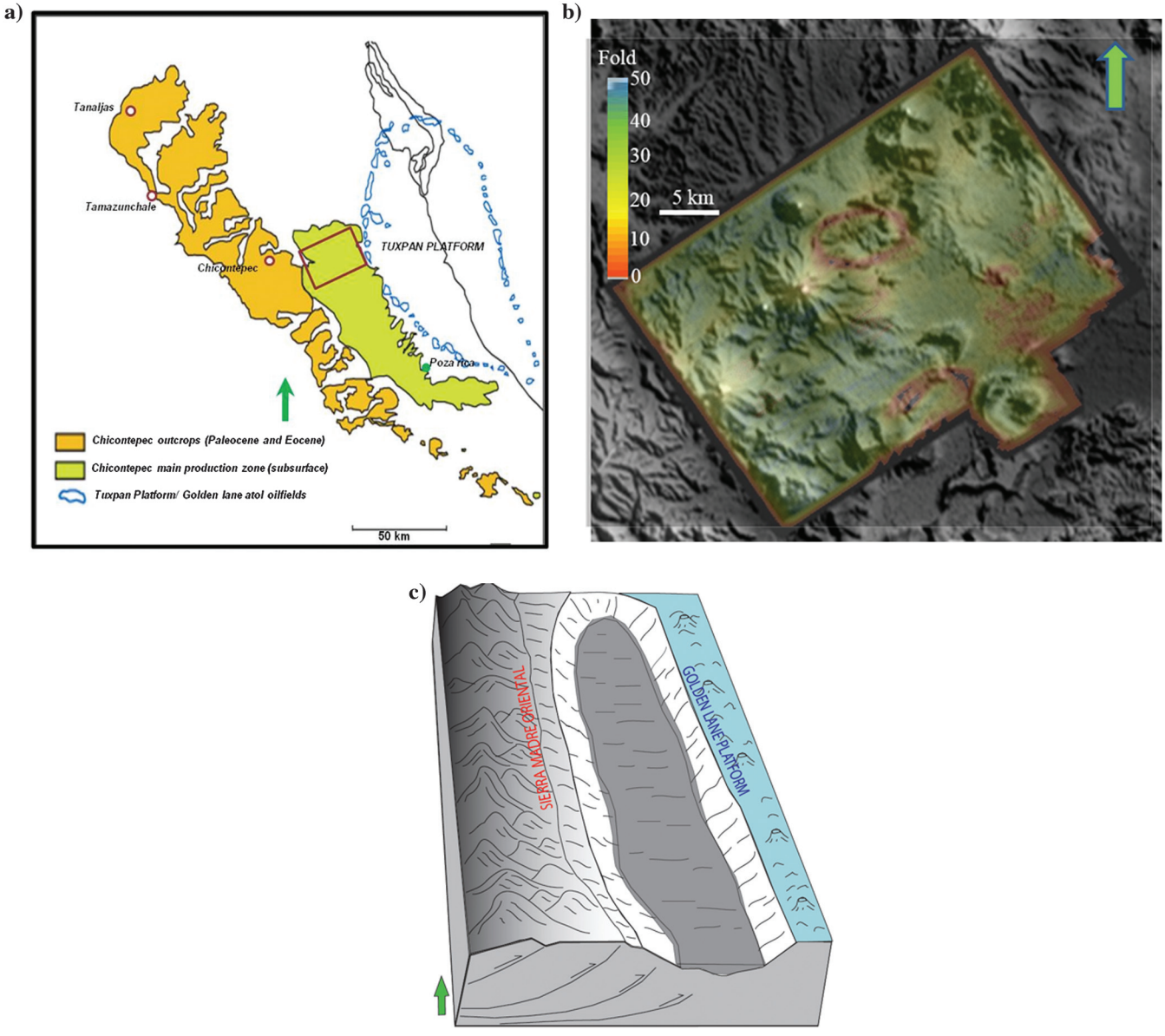

Figure 1. (a) Location map of the Chicontepec foredeep in east-central Mexico (modified after Bermúdez et al., 2006). The orange area indicates the foothill region of the SMO fold thrust belt. The red rectangle is the outline of the 3D seismic coverage within the northern part of the Chicontepec Basin, where this study is concentrated. (b) Digital elevation map blended with the seismic fold map. Several extrusive volcanic mounds can be observed throughout the survey area (modified from Pena et al., 2009). (c) Schematic diagram showing the Chicontepec foredeep forming an elongated trough between the SMO and the Golden Lane (Tuxpan) platform.

sections within the stratigraphic units. Then, we use the 3D seismic data volume to map the distribution of the best reservoir properties in 3D space. After preconditioning the seismic gathers, we obtain rock properties using prestack angle-dependent inversion, and map the potential reservoir bodies within each stratigraphic unit within our facies distribution framework. Finally, we compare the zones that have potential reservoirs from multiple stratigraphic units to the available production data to high grade areas of greater productivity.

Stratigraphic framework

Sarkar (2011) develops the stratigraphic framework in the northern part of the Chicontepec foredeep by integrating outcrop information with well-log correlation, chronostratigraphic calibration, seismic geomorphology, and core interpretation. The Chicontepec reservoir section has been subdivided into five stratigraphic units equivalent to global third-order sequences of Haq et al. (1987) (Figure 2). Deepwater facies distribution patterns within those stratigraphic units show two major flow directions that provide the sediments within the Chicontepec foredeep (Figure 3). The basin axis-parallel system consisting of multiple channels and amalgamated channel systems dominate the Upper Paleocene basal Chicontepec sequence, or unit A. The basin axis-perpendicular channel-fan systems and mass transport complexes originate from the SMO fold thrust belt as well as rivers or canyons passing through the SMO. Basin subsidence and sediment accumulation from the basin axis-perpendicular system are closely related to the tectonic activity that continued from Late Upper Paleocene to Early Eocene time. The basin axis-perpendicular system dominate the Early Eocene stratigraphic units, although the presence of axial flows gives rise to mixed depositional systems in several zones. The influence of axial channel systems progressively weakens toward the top of the Chicontepec strata. Within the uppermost zones of the Chicontepec reservoirs, especially in unit E (equivalent to third-order global sequence TA 2.9 of Haq et al., 1987), the proportion of finer clastics or clays increases, giving rise to poorer reservoirs. This stratigraphic system derived from this integrated study is different than the existing Chicontepec depositional concepts (Busch and Govela, 1978; Cheatwood and Guzmán, 2002; Abbaszadeh et al., 2003).

Petrophysical analysis

Petrophysical properties from well logs provide the basis to define rock types, reservoir zones, and mechanical properties that can be correlated to inverted surface seismic data showing their distribution in 3D space. Along with the petrophysical properties obtained directly from the well logs and core measurements (Table 1), we also analyze and derive rock properties, such as Lamé's parameters of rigidity μ, incompressibility λ, Young's modulus E, and Poisson's ratio ν. In the following sections, we discuss the most important petrophysical properties and their application in reservoir delineation.

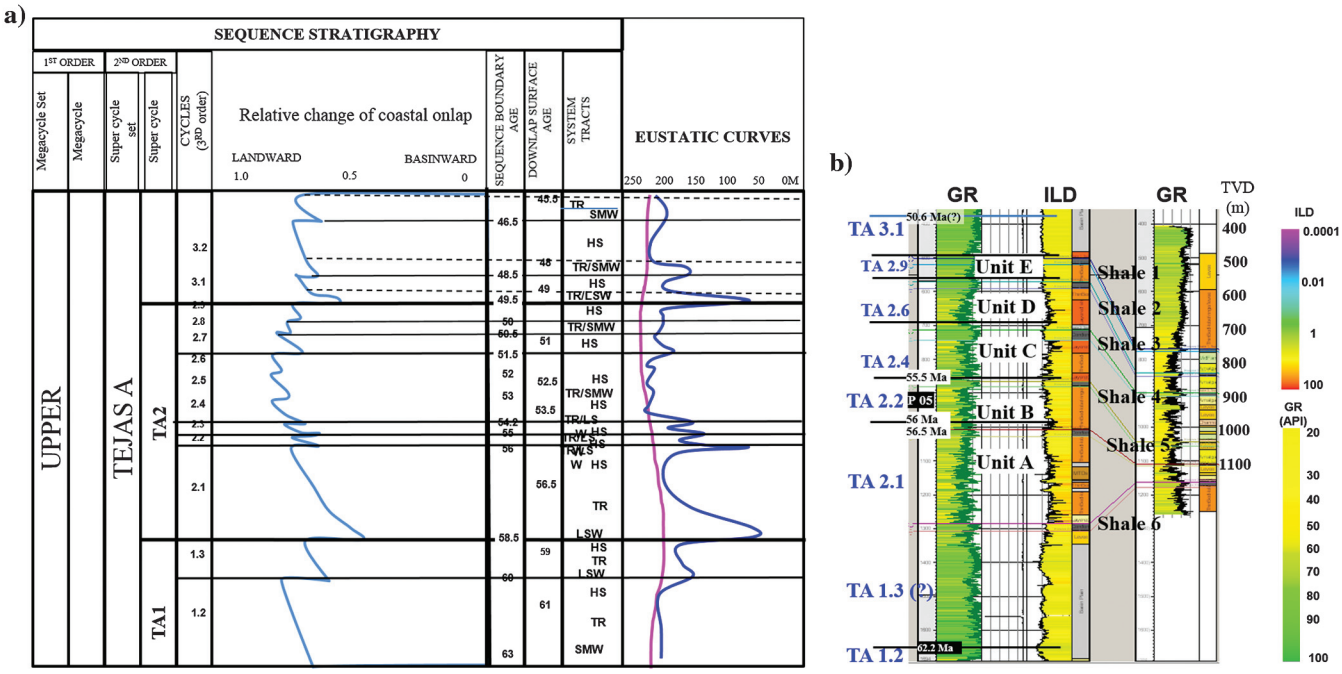

Figure 2. (a) Eustatic curves and global third-order sequences for the Upper Paleocene-Early Eocene (modified after Haq et al., 1987). (b) Six regionally extensive shale layers and possible condensed sections, identified from stratigraphic correlation that divides the Chicontepec reservoir section into five stratigraphic units labeled A-E. Using biostratigraphic records, the stratigraphic units can be correlated with global sequences TA 2.1, TA 2.2, TA 2.4, TA 2.6, and TA 2.9.

Gamma ray

Gamma-ray (GR) logs clearly demarcate the shale zones in between the reservoir units (Figure 4a), with a shale cutoff of GR < 55 for the best reservoir intervals. Carbonate rock fragments are a major constituent of this system. Because the GR count of carbonates is very low, GR logs alone are insufficient to identify good reservoirs.

V_P/V_S ratio

The V_P/V_S ratio has been used successfully to classify tight sand reservoirs (Rojas et al., 2005; Close et al., 2010; Valentin and Tatham, 2010). The V_P/V_S ratio shows moderate to high correlation with GR within a particular well, and it also defines the reservoir zones (Figure 4b). In more carbonate-rich reservoir intervals, the V_P/V_S ratio delineates the reservoir zone better than GR. Across the study area, the best productive reservoir zones fall within a V_P/V_S ratio of 1.7–1.94.

μ (rigidity), λ (incompressibility), and $\lambda\rho$-$\mu\rho$ crossplots

Goodway et al. (1997) show the value of μ (rigidity) and λ (incompressibility) in the identification of reservoir zones. The function λ indicates sensitivity to pore fluids, whereas μ and λ together serve as a lithology indicator. The value μ and λ can be calculated from the V_P, V_S, and density logs from the following equations:

$$\mu = \rho V_S^2, \tag{1}$$

and

$$\lambda = \rho V_P^2 - 2\rho V_S^2. \tag{2}$$

A primary objective is to obtain rock properties from seismic inversion. Debski and Tarantola (1995) and Gray and Andersen (2000) show that AVO inversion can accurately estimate two parameters $\lambda\rho$ and $\mu\rho$. The products $\lambda\rho$ and $\mu\rho$ can be accurately estimated from prestack seismic gathers and provide the same lithology discrimination as λ and μ.

Computing $\mu\rho$ and $\lambda\rho$ in several wells across the Chicontepec play from conventional logs shows $\mu\rho$ to be an excellent indicator of the calcilithite reservoir rocks (terminology from Folk, 1965) within the Chicontepec Formation (Figure 4c) because μ is directly related to the matrix composition. In contrast, the Chicontepec reservoirs are very tight and contain oil (mostly with no free gas), and λ is relatively insensitive to the reservoir zone (Figure 4d).

The two seismically measurable properties that best describe the productive zones within the Chicontepec reservoir interval are $\mu\rho$ and V_P/V_S. Crossplots between $\mu\rho$ and V_P/V_S ratio from 10 wells from different fields reveal the different trends of reservoir and

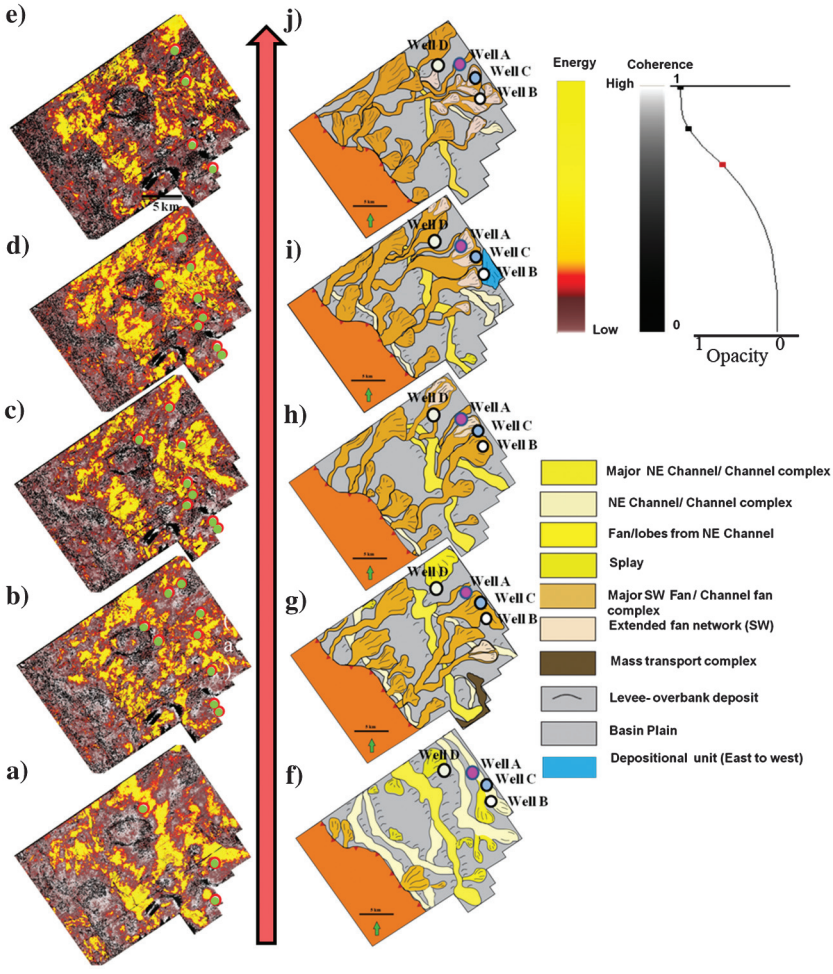

Figure 3. (a-e) Stratal slices along stratigraphic units A-E through coherent energy co-rendered with coherence volumes. Core locations used during interpretation are indicated by green circles. (f-j) Turbidite facies pattern within unit A-E (corresponding to a-e) based on seismic geomorphology combined with well control.

Table 1. List of well logs analyzed for the petrophysical analysis.

Total wells	GR	Density	P-wave sonic	S-wave sonic	Neutron porosity	Permeability	Core	Deep resistivity	Wells with all logs
100	80	35	51	11	20	35	11	25	3

nonreservoir rocks within the Chicontepec reservoir zone (Figure 5a). The range of $\mu\rho$ for delineating productive intervals varies between different stratigraphic units and shows an overall decrease in the mean value from lower to upper stratigraphic units (Figure 4c). This value varies between 18 and 34 GPa g/cm^3 for unit E, 22 and 38 GPa g/cm^3 for unit D, 23 and 42 GPa g/cm^3 for unit C, 25 and 45 GPa g/cm^3 for unit B, and 26 and 46 GPa g/cm^3 for unit A. The $\lambda\rho$ versus V_P/V_S crossplots from the same wells also show demarcation between reservoir and nonreservoir zones (Figure 5b). The $\lambda\rho$ value for the productive reservoir zones varies between 38 and 56 GPa g/cm^3 for stratigraphic unit A, 44 and 58 GPa g/cm^3 for unit B, 42 and 56 GPa g/cm^3 for unit C, and 33 and 53 GPa g/cm^3 for units D and E. The mean value of $\lambda\rho$ shows a decreas-

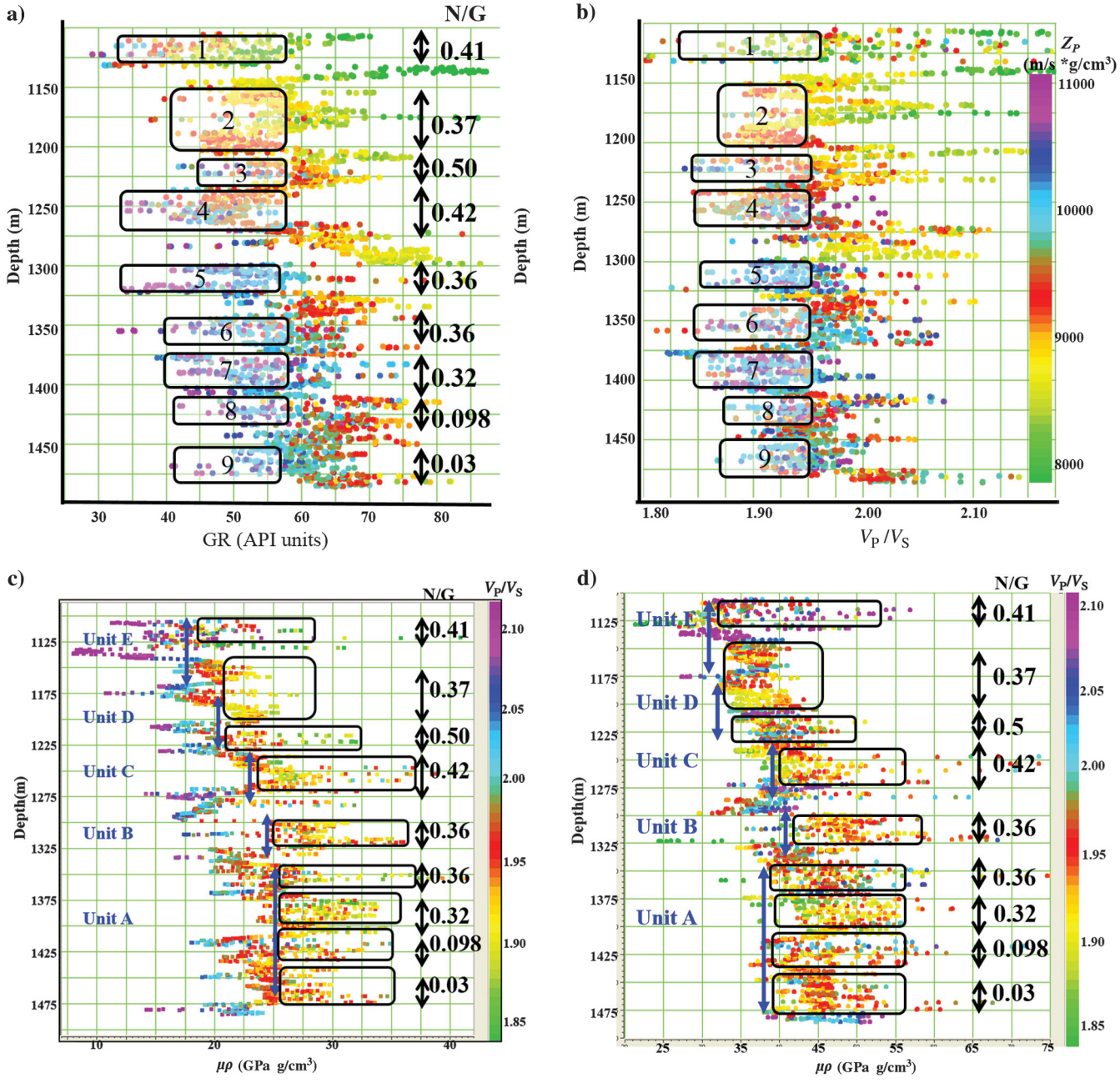

Figure 4. (a) Depth versus GR and (b) depth versus V_P/V_S plot, colored by P-impedance Z_P for well A (shown in Figure 3f–3j). Note the better definition of the reservoir units by relatively low values of GR and V_P/V_S ratio in those reservoir units. Higher impedance zones predominantly correspond to higher carbonate content. (c) The $\mu\rho$ versus depth and (d) $\lambda\rho$ versus depth plot from the same well colored with V_P/V_S ratio. Note, in (c and d), blue arrows indicate the stratigraphic units within Chicontepec reservoir zone as shown in Figures 2 and 3, the changing boundary values of $\lambda\rho$ from bottom to top stratigraphic units. Black rectangles indicate the reservoir units and their N/G ratio (from postdrill information) within the stratigraphic units. The reservoir zones less than 1400 m have low N/G ratio (less than 0.1) due to very low porosity and permeability.

ing trend from units A to E. Our analysis indicates that a few high carbonate-prone poor reservoir areas can be eliminated for values of $\lambda\rho > 58$ GPa g/cm^3, where V_P/V_S <1.94 (Figure 5b). Most of these areas also fall within an acceptable range of $\mu\rho$ for the reservoir zone (18–46 GPa g/cm^3). Qualitatively delineating the most productive zones using the boundary values for these three parameters ($\lambda\rho$, $\mu\rho$, and V_P/V_S ratio) provides the best result. Because $(\lambda\rho/\mu\rho) = (V_P^2/V_S^2) - 2$, the V_P/V_S ratio can be directly correlated to the points within $\lambda\rho$-$\mu\rho$ space. Plotting the points in $\lambda\rho$-$\mu\rho$ space and coloring with the GR values provide a broad idea

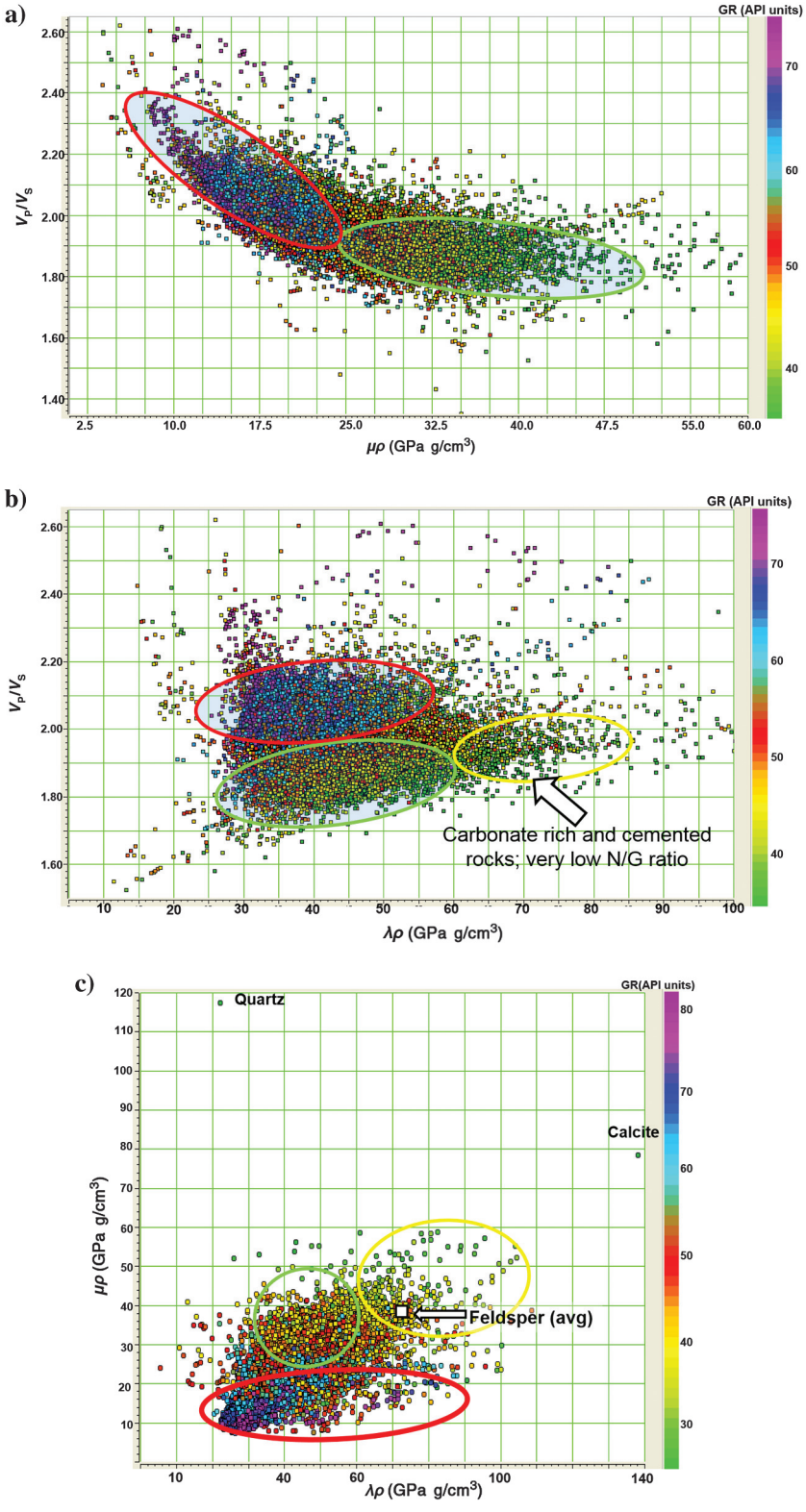

Figure 5. (a) Crossplot between $\mu\rho$ and V_P/V_S ratio from 10 wells across the northern Chicontepec Basin, colored by GR. The green ellipse indicates reservoir rocks (lower GR values), and red ellipse indicates nonproductive rocks (higher GR values). Note the trends of the points within green and red ellipses have different slopes. (b) Crossplot between $\lambda\rho$ and V_P/V_S ratio from 10 wells across the northern Chicontepec Basin, colored by GR. (c) The $\lambda\rho$-$\mu\rho$ crossplot colored by GR, from the points within the Chicontepec reservoir interval from multiple wells across the field along with values for pure quartz, calcite, and feldspar (average). For (b and c), green ellipse indicates values from the reservoir units, whereas the red ellipse defines the points from nonproductive units. Low GR points within the yellow ellipse are from very low N/G ratio carbonate rich cemented, poor reservoir rocks have a value of $\lambda\rho > 60$ GPa g/cm^3.

about the reservoir zone, and we can demarcate the points with the boundary values discussed above (Figure 5c). Within a stratigraphic unit, the better reservoir zones show higher $\mu\rho$ and lower $\lambda\rho$. To conceptualize the effect of the three major constituents of the rocks; calcite and quartz, feldspar within the $\lambda\rho$-$\mu\rho$ space, and their values are plotted alongside the points from the reservoir zones. This plot indicates an overall trend toward calcite, which conforms to the fact that calcite rock fragments and cement are the dominant constituent of these rocks. However, at the same time, the best reservoir zones have a trend toward quartz abundance. Laboratory analyses of core samples indicate that porosity in the Chicontepec reservoirs is inversely proportional to the calcite percentage in the rock, whereas decrease in calcite/quartz ratio can be correlated with higher porosity within the rock (Figure 6).

Neutron porosity

Because a neutron porosity log is a measure of hydrogen concentration (response primarily comes from the pore fluids of the formation), it shows high values in shales and clay rich areas within the reservoir zones in the Chicontepec Formation (Figure 7a) mainly due to bound water rather than effective porosity. Neutron porosity is also sensitive to water-filled and nonconnected intragranular pores from the carbonate rock fragments. Nevertheless, neutron porosity is one of the best tools to estimate the relative porosities within the Chicontepec reservoir units, and it correlates reasonably well with the reservoir facies demarcated by $\mu\rho$ and V_P/V_S ratio, where it distinguishes between reservoir and nonreservoir areas (Figure 7b). Neutron porosity values range between 5% and 30% for the potential productive facies.

The zones marked in Figure 5c for best, poor, and nonreservoir rocks are further supported by a $\lambda\rho$-$\mu\rho$ crossplot from three of the wells in Figure 5c (wells A-C in Figure 3) colored with neutron porosity (%, Figure 7c) and permeability (mD, Figure 7d). The shaly nonreservoir zones show highest neutron porosity and lowest permeability. The good reservoir rocks represented by green ellipse in Figure 7c and 7d show moderate neutron porosity and 80% of the points fall within 0.1–0.5 mD permeability values, whereas poor reservoir rocks marked by the yellow ellipse show lowest neutron porosity and very low permeability. Dividing the $\lambda\rho$-$\mu\rho$ crossplot in Figure 8 within the stratigraphic units (A-E) supports the $\mu\rho$ values corresponding to the productive zones within those units.

Young's modulus and Poisson's ratio

Oil production from tight Chicontepec reservoirs requires extensive hydraulic fracturing and stimulation. The Chicontepec rocks are assumed to be homogeneous, isotropic, and elastic. Along with the in situ stress field, the rock mechanics and brittleness are generally defined by Young's modulus E and Poisson's ratio ν. A range of values E and ν defines the more brittle reservoir zones for tight sand and shale gas reservoirs (Grigg, 2004).

Young's modulus E is a measure of elastic stiffness and is indicative of mechanical strength of rocks; Young's modulus is used by drilling engineers to design the wellbore. Therefore, predrill prediction of E is extremely important for safe and successful well design as well as defining the limits for hydraulic fracturing. Higher Young's modulus E indicates higher mechanical stiffness, which in turn can be positively correlated with brittleness.

Poisson's ratio ν measurement is directly related to the in situ stress as well as applied stress. The relationship between the vertical maximum matrix stress σ_V and the horizontal stresses (where the horizontal stresses are considered to be equal) is given by $\sigma_{H\,\max} = \sigma_{H\,\min} = (v/[1-v])\sigma_V$. Poisson's ratio for petroleum reservoirs ranges from 0.10 to 0.35 (Daniel and Dowell, 1980). The E and ν values for quartz are, respectively, 95.75 and 0.08 GPa, whereas those values for calcite are, respectively, 76.5 and 0.32 GPa. An increase in quartz and a decrease in calcite, corresponding to an increase of the Young's modulus and decrease of the Poisson's ratio, improves the quality of the Chicontepec reservoir. Quartz is much more frackable than calcite, such that better reservoir zones within the Chicontepec reservoir have a higher quartz content.

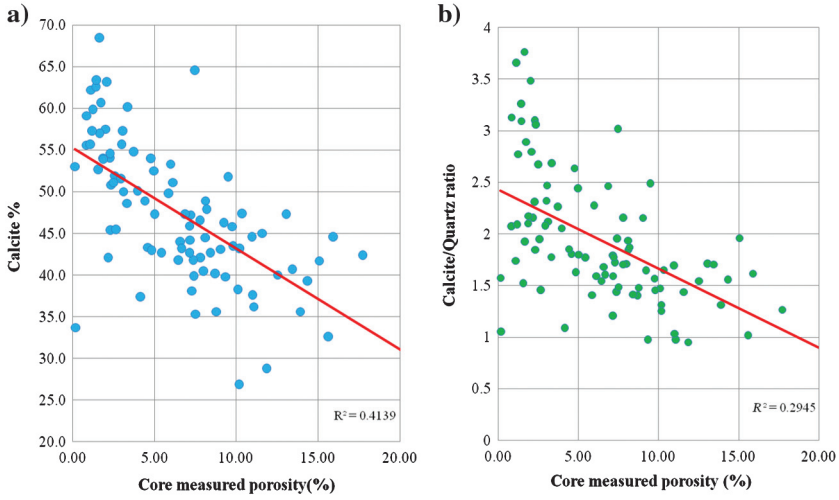

Figure 6. Crossplot between core measured porosity, and (a) calcite weight percent, and (b) against calcite/quartz ratio on data from multiple wells within Chicontepec reservoir rocks in the study area. Note the low-porosity areas correspond to the higher calcite and high-calcite/quartz ratio. Porosity increases with a decrease in calcite content in (a), whereas in (b) lower quartz/calcite ratio exhibits a higher porosity trend.

E and ν can be related to μ (rigidity) by

$$\frac{E}{1+\upsilon} = 2\mu, \tag{3}$$

which indicates that μ is directly proportional to E and inversely proportional to ν. Poisson's ratio ν is a function of the V_P/V_S ratio by the following equation:

$$\upsilon = 0.5\frac{\left(\frac{V_P}{V_S}\right)^2 - 2}{\left(\frac{V_P}{V_S}\right)^2 - 1}. \tag{4}$$

Reservoir intervals of V_P/V_S: 1.7–1.94 correspond to ν values between 0.27 and 0.31 and E values 30–50. Thus, petrophysical analysis indicates that the best reservoir zones of Chicontepec sandstone are among the most suitable rocks for hydraulic fracturing. Crossplotting E versus ν demarcates the best frackable zones within the reservoir (Figure 9).

In summary, petrophysical analysis indicates that the Chicontepec reservoir section can be divided into relatively better reservoir, poor reservoir, and shaly nonreservoir zones, which are clearly defined in the $\lambda\rho$-$\mu\rho$ space. Highly cemented poor reservoir zones correspond to high calcite and high calcite to quartz ratio within the rock. The best reservoir definition can be obtained from $\mu\rho$ and V_P/V_S ratio along with $\lambda\rho$ values, where a unique range of $\mu\rho$ and $\lambda\rho$ values characterizes each stratigraphic unit within the reservoir zone. High E and moderate ν values indicating potential "frackable" zones (Grigg, 2004) correspond to the relatively better reservoir areas defined from the petrophysical analysis.

Seismic data analysis

Analysis of the petrophysical properties of the Chicontepec reservoir rocks revealed that the best properties for delineating prospective intervals within the Chicontepec reservoirs are the rigidity μ, the V_P/V_S ratio, and the best, poor, and nonreservoir zones can be designated clearly in the $\lambda\rho$-$\mu\rho$ space. To estimate surface seismic data for these properties (Figure 10), we performed simultaneous angle-dependent inversion (Hampson et al., 2005) on the preconditioned prestack common reflection point gathers. The preconditioned prestack gathers were obtained after reprocessing of the prestack seismic data with velocity analysis on fine grid (375 × 375 m) as well as ap-

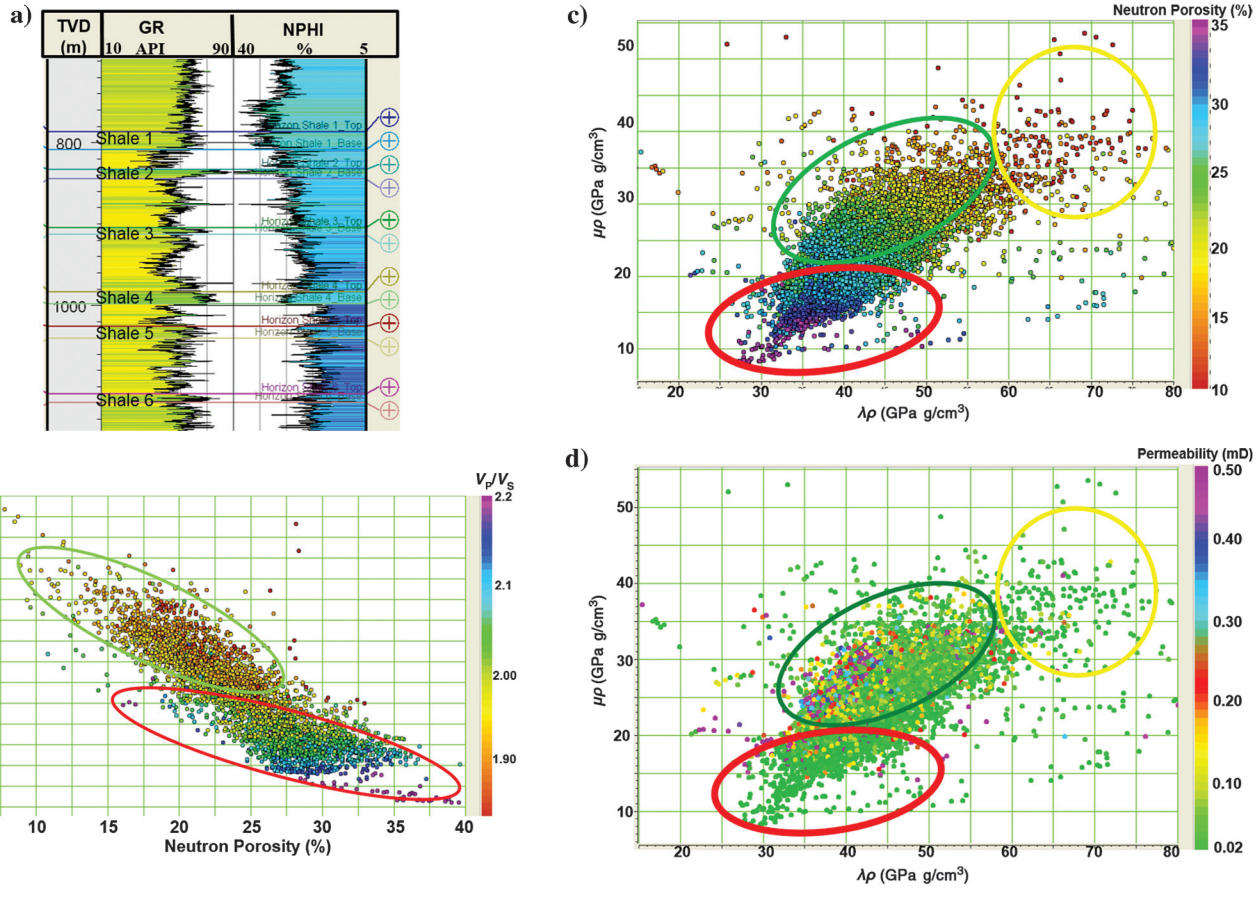

Figure 7. (a) GR and neutron porosity (NPHI) logs in the Chicontepec reservoir interval from well A. With data from wells A-C shown in Figure 3, (b) crossplot between $\mu\rho$ and neutron porosity colored with V_P/V_S ratio; crossplot between $\lambda\rho$ and $\mu\rho$ colored with (c) neutron porosity (%) and (d) permeability (mD) values. The good, poor, and nonreservoir zones shown by green, yellow, and red ellipses, for (c and d), these zones correspond to zones shown in Figure 5.

plication of structure oriented filtering after prestack migration (Sarkar, 2011, 2013).

We selected 20 wells representing good and bad production across the seismic survey to tie the seismic data and provide the low-frequency Z_P and Z_S components not measured by the seismic experiment. Ideally, each of the wells has S-wave (or dipole sonic) as well as P-wave logs. Because all of the wells did not have dipole sonic information, we derived a relationship between P- and S-wave slowness from multiple wells with dipole sonic logs across the northern part of the Chicontepec Basin. We applied this relationship to the wells that did not have S-sonic log.

Angle-dependent wavelets were extracted for each of three limited angle gathers (near-angle stack: 0°–11°, mid-angle stack: 12°–22°, and far-angle stack: 23°–33°) by tying the seismic gathers to the wells with synthetic

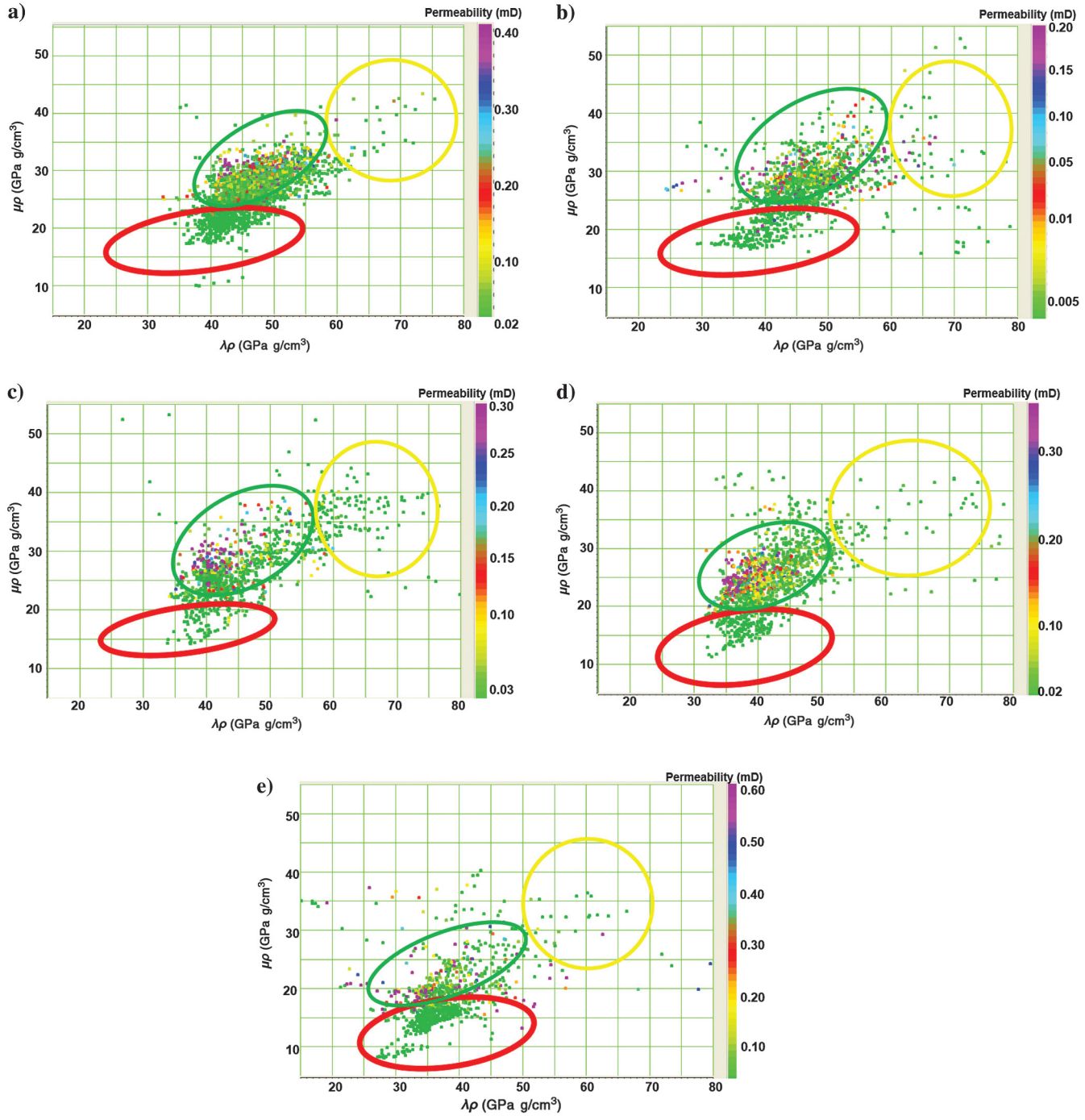

Figure 8. (a-e) Represent $\lambda\rho$-$\mu\rho$ crossplots corresponding to stratigraphic units A-E, respectively, colored by log permeability values from the same wells as in Figure 7d. The green ellipse in each of the panels shows ranges of $\mu\rho$ values corresponding to the stratigraphic unit for better reservoir zones. Red and yellow ellipses in each of the figures demarcate shaly nonreservoir and highly cemented poor reservoir zones, respectively.

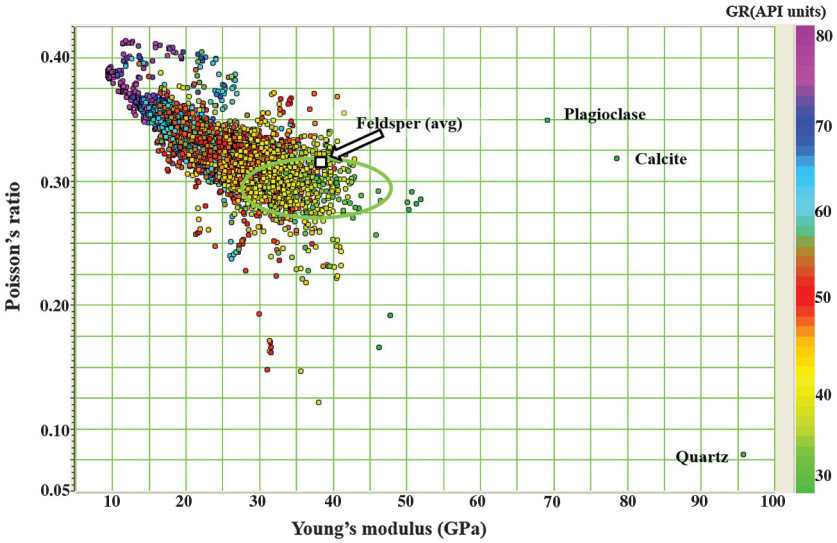

Figure 9. The E versus ν crossplot colored by GR from wells A-C (shown in Figure 3) along with the corresponding values of pure quartz, calcite, plagioclase feldspar, and average feldspar. Green ellipse indicates reservoir rocks in wells A-C and falls within the productive reservoir zone shown in Figure 5c. This zone also correlates to more brittle units (Grigg, 2004).

seismograms. The wells tie well within the Chicontepec interval with correlation coefficients 73%–95%. Simultaneous inversion performed on the prestack gathers resulted in P- impedance Z_P and S-impedance Z_S volumes (Figure 11).

Interpretation

Volumetric prediction of rock type

The previous well-log rock properties analysis (Figure 5) showed that the productive zones within the Chicontepec interval fell within a specific range of $\mu\rho$, $\lambda\rho$, and V_P/V_S values. Here, we compute $\mu\rho$ and $\lambda\rho$ volumes from seismic inversion products Z_P and Z_S using the following equations:

$$\mu\rho = Z_S^2, \tag{5}$$

$$\lambda\rho = Z_P^2 - 2Z_S^2. \tag{6}$$

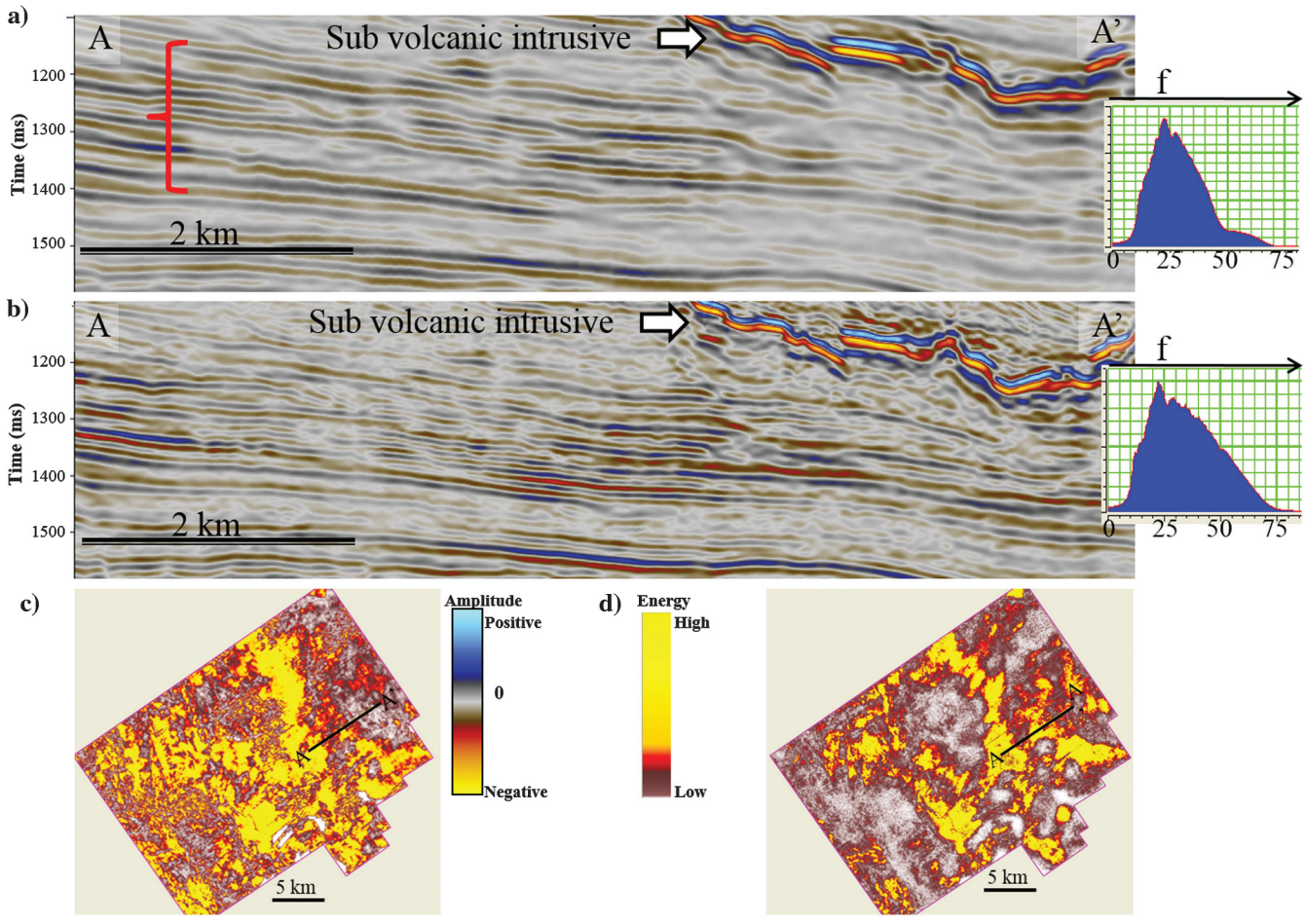

Figure 10. Example of (a) original prestack time migrated vertical seismic amplitude section and (b) the same section after performing residual velocity analysis. Note the improved stratal definition within the Chicontepec interval demarcated by the red bracket and also below the shallow volcanic body. The frequency spectra corresponding to each volume indicates significant frequency enhancement. (c and d) Equivalent coherent energy slices along the black horizon in (a and b).

The data points from these computed volumes show a similar distribution in $\lambda\rho$-$\mu\rho$ space to the well data in Figure 5c within the Chicontepec Formation (Figure 12). This similarity is also an indicator for the quality of the inversion process.

Spatial correlation of rock type and facies distributions

Through the use of 3D seismic visualization, we can highlight voxels having $\lambda\rho$-$\mu\rho$ values corresponding to potential reservoir zones. Figures 13 and 14 show each of the

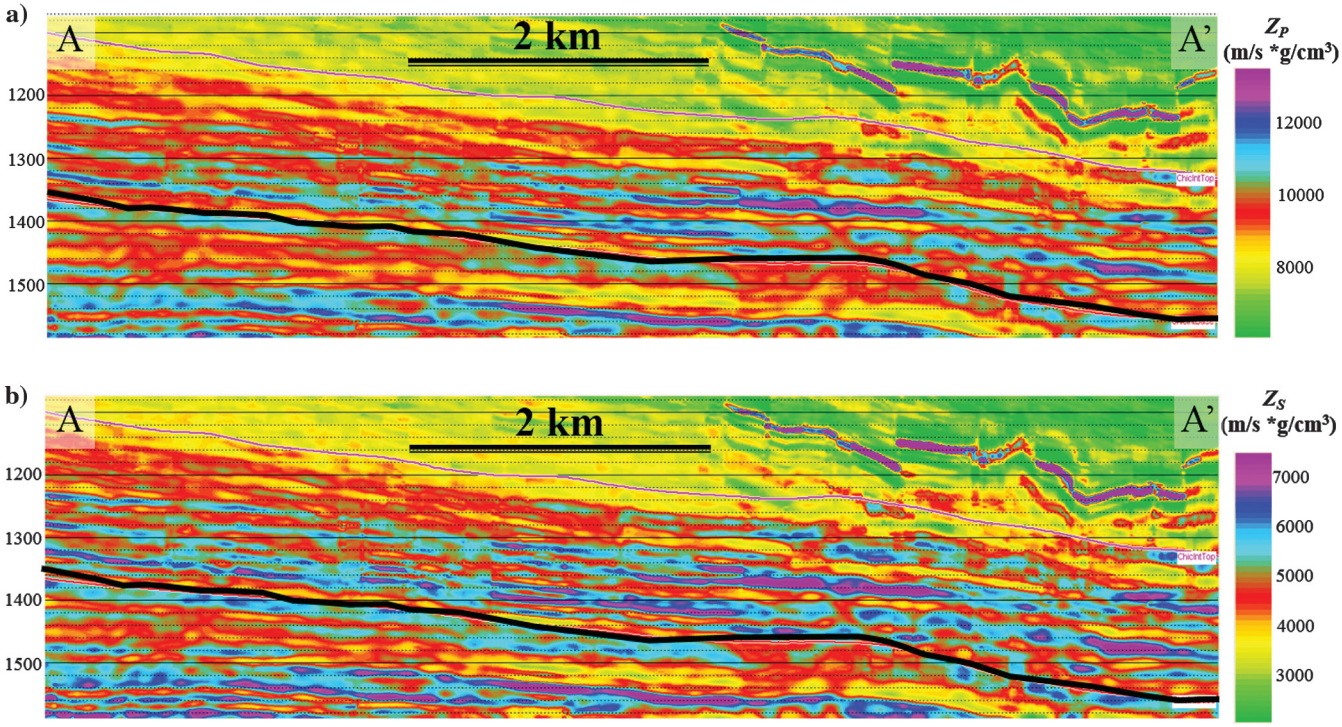

Figure 11. Vertical slices along AA′ shown in Figure 10c and 10d through the inverted Z_P and Z_S volumes.

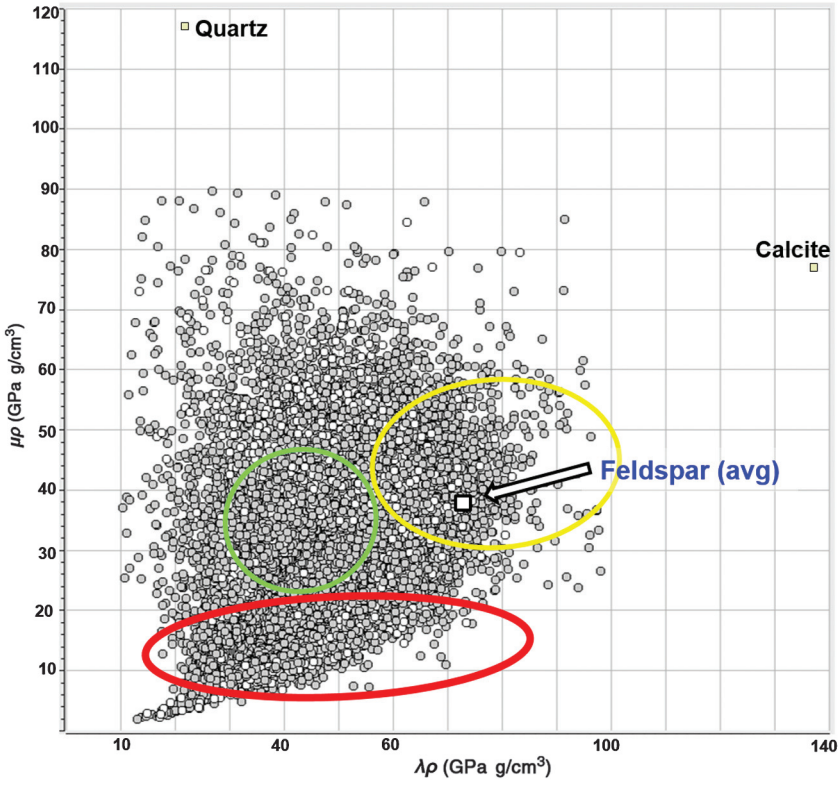

Figure 12. Seismically estimated $\lambda\rho$-$\mu\rho$ crossplot from points within the Chicontepec reservoir interval plotted using the same scale as in Figure 5c with the values of pure quartz, calcite, and average feldspar. The lithology polygons from Figure 12 have been transferred to this crossplot.

five stratigraphic units shown in Figures 2 and 3. We also correlated the seismic geomorphologic interpretation with the trends from seismic inversion results in Figure 15.

Delineating potential prospective zones with visualization techniques

Transferring values from Figure 12, we analyzed the prospective areas within a stratigraphic unit along stratal slices, where $\lambda\rho$, $\mu\rho$, and V_P/V_S ratio values are plotted from the inverted rock property cubes. Using transparency applied to $\lambda\rho$-$\mu\rho$ crossplots for the stratigraphic units we highlighted prospective $\lambda\rho$-$\mu\rho$ ranges that we analyzed from the petrophysical analysis, which corresponds with the V_P/V_S ratio range determined for the good reservoir zone (1.7–1.94; Figures 13 and 14). The zones with poor seismic quality

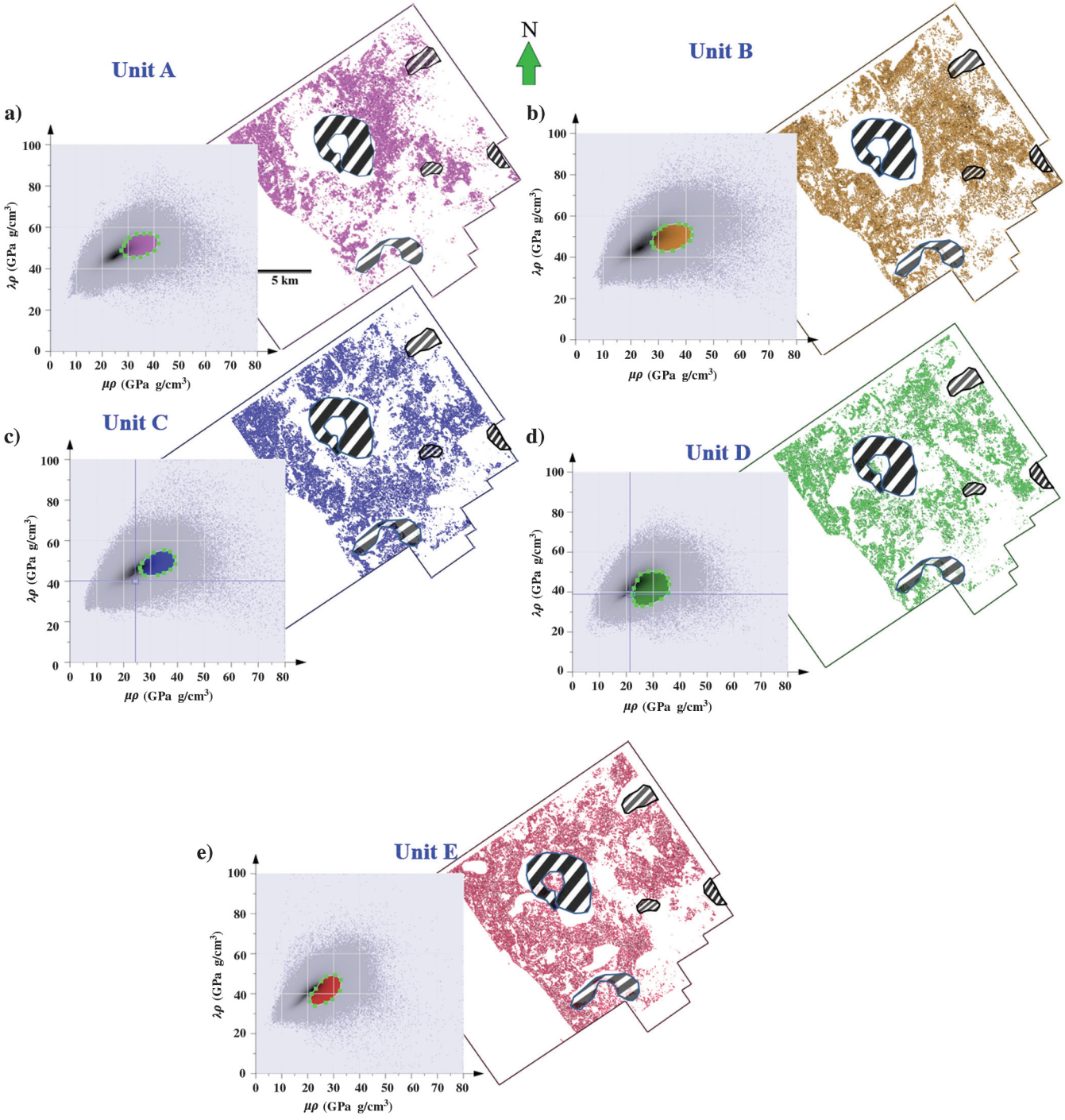

Figure 13. (a-e) The potential pay zone map, respectively, for stratigraphic units A-E obtained from the prestack inversion driven $\lambda\rho$-$\mu\rho$ volumes and using the transparency applied to the $\lambda\rho$-$\mu\rho$ crossplot. The grayed areas in the color bars in (a-e) represent the zones that were made transparent to display the prospective areas. The cross-hatched zones indicate poor seismic coverage areas.

(Figure 1b) are excluded from this analysis to reduce uncertainty.

We superimposed the potential pay zone maps for the stratigraphic units A–E from Figure 13 on the facies distribution maps (from Figure 3) to relate the potential reservoir distribution with respect to the interpreted deepwater architectural elements (Figure 14). The reasonably good correlation of the potential pay zones with the turbidite facies units validates the stratigraphic analysis and the reservoir characterization process. Some of the architectural elements show lack of continuity in the reservoir zone across them indicative of the character of the Chicontepec reservoirs spread as several small fields with little lateral continuity. One of the possible reasons is lateral variation in carbonate, clay content, and cementation due to complex interaction of several flows from different directions.

Correlation with production

The best way to evaluate the prospective zones interpreted from the seismic reservoir characterization process is to compare with the cumulative production data available. We drew polygons on each stratal slice shown in Figure 13 encompassing the potential pay zones. Polygons corresponding to each stratigraphic unit are represented by a unique color. Figure 15 shows areas in green, where at least four polygons from the different stratigraphic zones overlap. These zones with green polygons should coincide with better cumulative production areas, where we have available production information and represent the zones of potential "sweets spots." Because the wells started operating between 1969 and 2008, a good estimate of production is the cumulative production of the first six months, plotted as yellow circles,

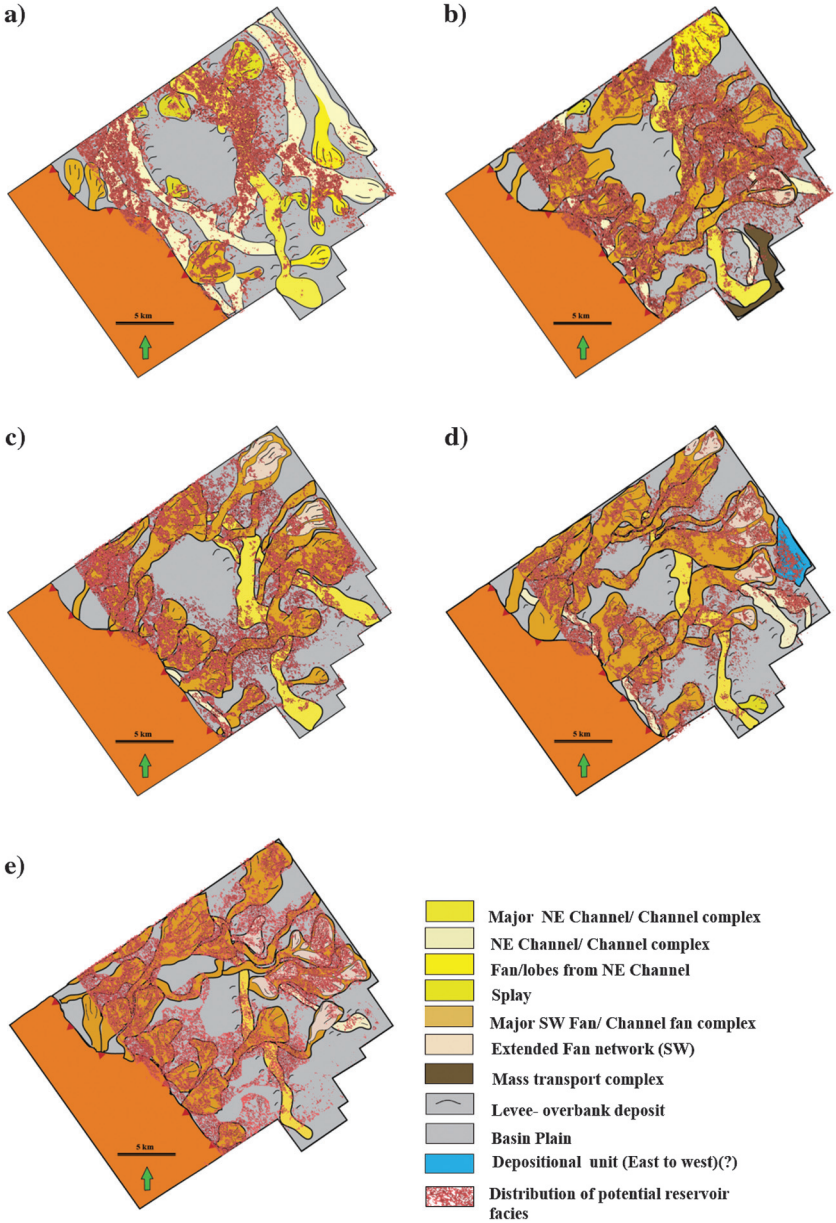

Figure 14. (a-e) Distribution of potential good reservoir facies (shown in red points) from Figures 13 plotted using transparency against the interpreted deepwater facies distribution maps along stratigraphic units A-E shown in Figure 3.

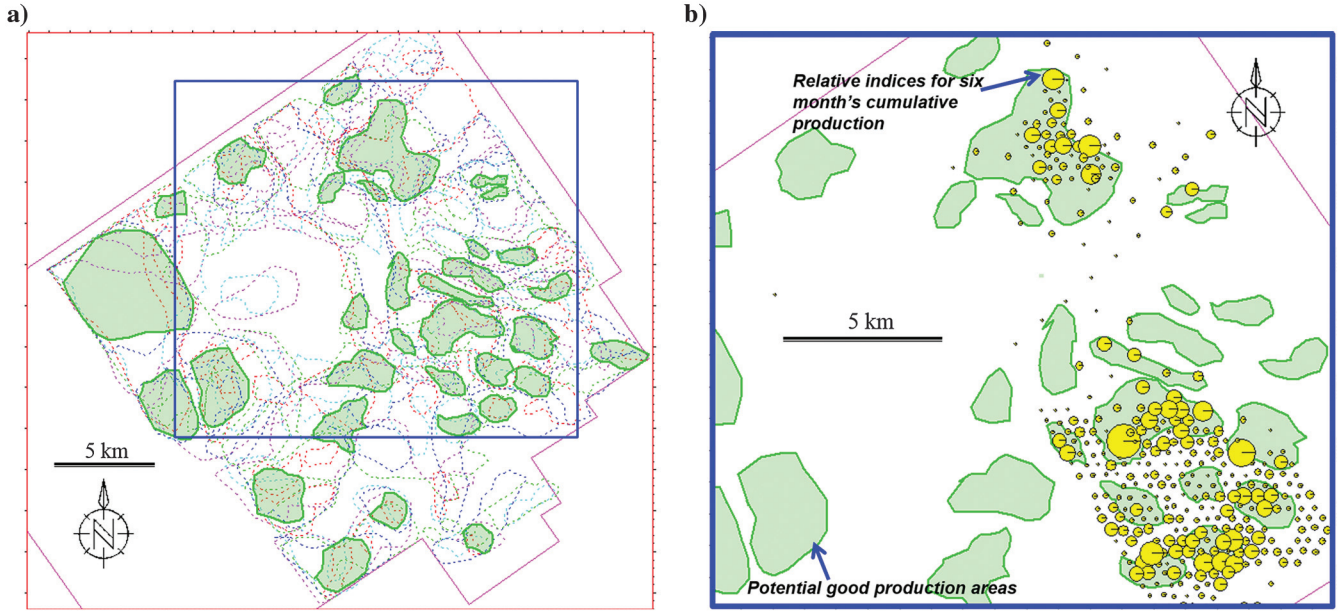

Figure 15. (a) Potential stacked pay obtained by projecting prospective polygons from all of the stratigraphic units. The green polygons indicate at least four levels of stacked pay. (b) Magnified blue rectangle area of predicted pay shown in Figure 15a plotted against six month's cumulative production. (Scaled production shown due to data sensitivity). The magenta lines indicate survey boundary.

where the radius of the circle is directly proportional to the first six months of production.

Note the overlap of the green polygons with the first six months of relative cumulative production. Most of the areas with well information coincide with the wells demonstrating better production (Figure 15b).

Conclusions

Seismic reservoir characterization has potential to significantly improve the understanding of the complex, tight, and mineralogically immature Chicontepec oil reservoirs. A similar methodology can be adopted for other tight reservoirs as well. Integration of seismic geomorphology with stratigraphic correlation constrained by chronostratigraphic records showed the Chicontepec interval in the northern part of the Chicontepec Basin to consist of five stratigraphic units, equivalent to third-order global stratigraphic sequences. The deep-water patterns within these stratigraphic units revealed complex interaction between axis-parallel and axis-perpendicular flow within the elongated foreland basin. Petrophysical analysis indicates the productive interval within a small window in $\lambda\rho$-$\mu\rho$ space, corresponding to rock types with good brittleness. Residual velocity analysis and application of structure-oriented filtering were key to improve vertical resolution and the signal-to-noise ratio of the prestack gathers. Calibration of crossplots of prestack inversion derived $\lambda\rho$-$\mu\rho$, $\lambda\rho$-V_P/V_S, and $\mu\rho$-V_P/V_S volumes, and the petrophysical crossplot analysis provides a volumetric estimation of rock type, which allowed the differentiation of shales and highly cemented sandstone from the less cemented reservoir sandstone. Further linkage of these rock types with the seismic geomorphology and facies distribution maps provides a means to extrapolate currently productive areas beyond the well control. The final product is a predicted stacked pay map showing four or more potential reservoir units that can be used statistically to reduce risk and update statistics with more drilling.

Acknowledgments

The authors acknowledge Pemex and especially J. Berlanga for providing the data and their facilities for educational purposes. Special thanks to S. Chavez Perez of IMP for his enormous support and guidance. The authors would like to acknowledge CGG GeoSoftware for its donation of H. Russell, which was used for prestack inversion, and Schlumberger for providing the Petrel software, which was used for seismic interpretation. The financial support for this work was provided by industry support of the Attribute-Assisted Seismic Processing and Interpretation (AASPI) Consortium at the University of Oklahoma. Seismic attributes were generated using the AASPI Consortium software.

References

Abbaszadeh, M., T. Shimamoto, F. M. Sandria, D. H. Zamora Guerrero, and F. Rodriguez de la Garza, 2003, Integrated geostatistical reservoir characterization of turbidite sandstone deposits in Chicontepec Basin, Gulf of Mexico: Proceedings of the Society of Petroleum Engineers Annual Technical Conference and Exhibition, SPE paper 84052, 15.

Bermúdez, J. C., J. Araujo-Mendieta, M. Cruz-Hernández, H. Salazar-Soto, S. Brizuela-Mundo, S. Ferral-Ortega, and O. Salas-Ramírez, 2006, Diagenetic history of the turbiditic litharenites of the Chicontepec Formation,

northern Veracruz: Controls on the secondary porosity for hydrocarbon emplacement: Gulf Coast Association of Geological Societies Transactions, **56**, 65–72.

Busch, D. A., and S. A. Govela, 1978, Stratigraphy and structure of Chicontepec turbidites, southeastern Tampico-Misantla Basin: AAPG Bulletin, **62**, 235–246.

Cheatwood, C. J., and A. E. Guzmán, 2002, Comparison of reservoir properties and development history — Spraberry trend field, west Texas and Chicontepec field, Mexico: Proceedings SPE International Petroleum Conference and Exhibition, SPE Paper 74407, 19.

Close, D., S. Stirling, D. Cho, and F. Horn, 2010, Tight gas geophysics: AVO inversion for reservoir characterization: CSEG Recorder, **35**, 28–35.

Cossey, S. P. J., 2008, Debrites in the Chicontepec Formation, Tetlahuatl, Mexico, *in* T. H. Nilsen, R. D. Shew, G. S. Steffens, and J. R. J. Studlick, eds., Atlas of deepwater outcrops: AAPG Studies in Geology 56, 231–234.

Daniel, G., and J. H. Dowell, 1980, Fundamentals of fracturing: Proceedings of the SPE Cotton Valley Symposium, SPE Paper 9064-MS, 8.

Debski, W., and A. Tarantola, 1995, Information on elastic parameters obtained from the amplitudes of reflected waves: Geophysics, **60**, 1426–1436, doi: 10.1190/1.1443877.

Donnelly, J., 2009, Mexico's challenge: Journal of Petroleum Technology, **62**, 16.

Folk, R. L., 1965, Petrology of sedimentary rocks: Hemphill Publishing Company.

Geetan, R., B. Hornby, and R. Wardhana, 2011, Seismic technologies for unconventional reservoir characterization: Wamsutter field case study: Annual Convention and Exhibition, AAPG, Abstract, Search and Discovery article #110159.

Goodway, B., T. Chen, and J. Downton, 1997, Improved AVO fluid detection and lithology discrimination using Lamé petrophysical parameters; "$\lambda\rho$", "$\mu\rho$," & "λ/μ fluid stack," from P and S inversions: 67th Annual International Meeting, SEG, Expanded Abstracts, 183–186.

Gray, F. D., and E. C. Andersen, 2000, Case histories: Inversion for rock properties: 62nd Annual International Conference and Exhibition, EAGE, Extended Abstracts, 4.

Grigg, M., 2004, Emphasis on mineralogy and basin stress for gas shale exploration: Presented at the SPE Meeting on Gas Shale Technology Exchange.

Hampson, D. P., B. H. Russell, and B. Bankhead, 2005, Simultaneous inversion of pre-stack seismic data: 75th Annual International Meeting, SEG, Expanded Abstracts, 633–637.

Haq, B. U., J. Hardenbol, and P. R. Vail, 1987, Chronology of fluctuating sea levels since the Triassic: Science, **235**, 1156–1166.

Pena, V., S. Chávez–Pérez, M. Vázquez-García, and K. J. Marfurt, 2009, Impact of shallow volcanics on seismic data quality in Chicontepec Basin, Mexico: The Leading Edge, **28**, 674–679.

Rojas, E., T. L. Davis, M. Batzle, and M. Prasad, 2005, V_P/V_S ratio sensitivity to pressure, fluid, and lithology changes in tight gas sandstones: 75th Annual International Meeting, SEG, Expanded Abstracts, 1401–1404.

Sarkar, S., 2011, Depositional history and reservoir characteristics of structurally confined foredeep turbidites, northern Chicontepec Basin: Ph.D. dissertation, University of Oklahoma.

Sarkar, S., 2013, Time to pick? No need to fear 'seismophobia': Geophysical Corner, AAPG Explorer.

Tobin, R.C., T. Mcclain, R. B. Lieber, A. Pzkan, L. A. Banfield, A. M. E. Marchand, and L. E. Mcrae, 2010, Reservoir quality modeling of tight-gas sands in Wamsutter field: Integration of diagenesis, petroleum systems, and production data: AAPG Bulletin, **94**, 1229–1266.

Valentin, D. A., and R. H. Tatham, 2010, Identifying Jurassic tight gas sands in the East Texas Basin with 3D-3C seismic data: 67th Annual International Meeting, SEG, Expanded Abstracts, 1620–1624.

Supratik Sarkar received a B.S. (2001) in geologic sciences from Jadapur University, India, an M.S. (2003) in applied geology from IIT Bombay, India, and a Ph.D. (2011) from the University of Oklahoma, USA. Since 2011, he has been working as an exploration geologist at Shell. He also worked at Reliance Industries Ltd. (E&P) and interned with Noble Energy Inc., and ConocoPhillips. His primary research interests include seismic geomorphology, deepwater depositional systems, and quantitative seismic interpretation.

Kurt. J. Marfurt began his geophysical career teaching geophysics and contributing to an industry-supported consortium on migration, inversion, and scattering (project MIDAS) at Columbia University's Henry Krumb School of Mines in New York City. In 1981, he joined Amoco's Tulsa Research Center and spent the next 18 years doing or leading research efforts in modeling, migration, signal analysis, basin analysis, seismic attribute analysis, reflection tomography, seismic inversion, and multicomponent data analysis. In 1999, he joined the University of Houston as a professor in the Department of Geosciences and as director of the Allied Geophysics Laboratories. He is currently a member of the Geophysical Societies of Tulsa and Houston, SEG, EAGE, AAPG, AGU, and SIAM, and he serves as editor of *Interpretation*. His current research activity includes prestack imaging, velocity analysis and inversion of converted waves, computer-assisted pattern recognition of geologic features on 3D seismic data, and interpreter-driven seismic processing. His research interests include seismic signal analysis, 3D seismic attributes, seismic velocity analysis, subsurface imaging, and multicomponent data analysis.

A biography and photograph of the other author are not available.